ON THE MOTION OF AUTOROTATING ELONGATED PRISMATIC BODIES

by

M. Poreh
and
R. N. Wray

for

National Bureau of Standards
Washington, D.C.
under
NBS Contract No. 1101-5064-35873

Fluid Dynamics and Diffusion Laboratory
College of Engineering
Colorado State University
Fort Collins, Colorado

August 1976

CER76-77MP-RNW6

ABSTRACT

ON THE MOTION OF AUTOROTATING ELONGATED PRISMATIC BODIES

The discussion presented in this study concerns the motion of elongated prismatic bodies and the forces induced on them by the relative wind. Two important dimensionless parameters which determine and characterize the motion of such bodies were identified--a dimensionless moment of inertia, I^* and the dimensionless rotational speed, nb/U.

Two stable modes of motion were observed for bodies with large I^*. When the flow is normal to the largest area of the body and no rotation exists, a translatory motion occurs. The drag coefficient in this case is of the order $C_D \approx 2$. When the body is oriented with its long axis normal to the flow and rotation exists around this axis, a steady autorotating mode occurs. In this mode one can distinguish between the following two extreme cases:

1. When nb/U is small, the average lift acting on the body is zero and the average drag can be calculated using the quasi-static approximation.
2. When nb/U is large the velocity field is modified and results in a slight change in the value of C_D from the value found for case 1. Furthermore, a very large lift coefficient due to a Magnus effect is generated, which is dependent upon nb/U.

In the case of small I^* the translatory mode is not stable and motion for the two cases of autorotation--nb/U small and large--is affected by I^* as well as by nb/U.

Wind-tunnel experiments by the authors and previous work by other investigators were used to estimate the drag and lift coefficients with different values of I^* and nb/U.

ACKNOWLEDGMENTS

This report is based in part on the M.S. Thesis of R. W. Wray. Dr. M. Poreh was the thesis advisor.

The authors wish to thank Dr. J. E. Cermak, Professor-in-Charge of Fluid Mechanics and Wind Engineering Program, for his help and advice during the project. The authors are also grateful to Dr. E. Simiu from the National Bureau of Standards and Dr. J. E. Castello from the Nuclear Regulatory Commission for their continuous stimulation and encouragement during the project. The help and contributions of Dr. W. Z. Sadeh, who lead the project in its early phases, is also gratefully acknowledged.

TABLE OF CONTENTS

LIST OF FIGURES

LIST OF SYMBOLS

Symbol	Definition
A^n	Body area projected normal to the flow
A^r	Body reference area
C_D	Drag coefficient
C_L	Lift coefficient
C_M	Moment coefficient
F	Aerodynamic force acting on body
I	Moment of inertia of body
I^*	Dimensionless moment of inertia
L	Characteristic length dimension
M	Aerodynamic moment acting on body
T_f	Time scale of flow
T_n	Time scale of rotation of the body
T_w	Time scale of oscillation of the body
U	Relative velocity between flow and body
W	Weight of the body
b	Width of rectangular body
f_i	Body force in the x_i direction
g	Acceleration due to gravity
h	Length of rectangular body
i	Subscript denoting direction (i = 1,2,3)
n	Rotation rate of body, (cycles/second)
t	Thickness of rectangular body
w	Instantaneous rotation of body
x_i	Coordinate system

Symbol	Definition
ρ_a	Density of fluid
ρ_b	Density of body
θ	Angle of incidence between body and flow
α	Angle of decent of autorotating body
$\bar{}$	Denotes averaged value

Chapter 1

INTRODUCTION

An important concern in the design of nuclear power plants is the possible impact and penetration of containment vessels by tornado propelled bodies. Currently, the motion and impact speed of such bodies cannot be satisfactorily ascertained. Part of the difficulty is in predicting the tornado velocity field which is space and time dependent. The exact shape and weight of such bodies is not known either. However, even when the velocity field is defined and typical bodies are chosen to represent tornado-generated missiles, the calculation of their motion remains complicated and uncertain.

Survey of the literature (Sadeh), shows that even the exact drag coefficients of simple bodies are not always known. Moreover, since the trajectory of a flying object which has six degrees of freedom is determined by all the forces and moments acting on it, knowledge of the drag coefficient alone is not sufficient for the calculation of the trajectory. In addition, flying objects, like a wood plank, could easily enter an autorotational or tumbling mode of motion, which drastically affects the trajectory.

The initial objective of this study was to determine, by wind-tunnel tests, some drag and lift coefficients of typical bodies which might become airborne in tornados. It became apparent, however, that the exact determination of these coefficients is of secondary significance as the variation in the projected areas due to the change of orientation of such bodies is manyfold larger. Attention is therefore focused in this study on autorotating elongated bodies,

particularly wood planks. The question of whether it is possible to describe the motion of such bodies by the motion of a material point on which average drag and lift forces are exerted, is studied. The values of the coefficients which have to be used in such a procedure are also investigated.

Chapter 2

ON THE MOTION OF FREE ELONGATED PRISMATIC BODIES

The motion of a free body can be described by six governing equations which represent the six degrees of freedom in translation and rotation, as shown in Fig. 2.1.

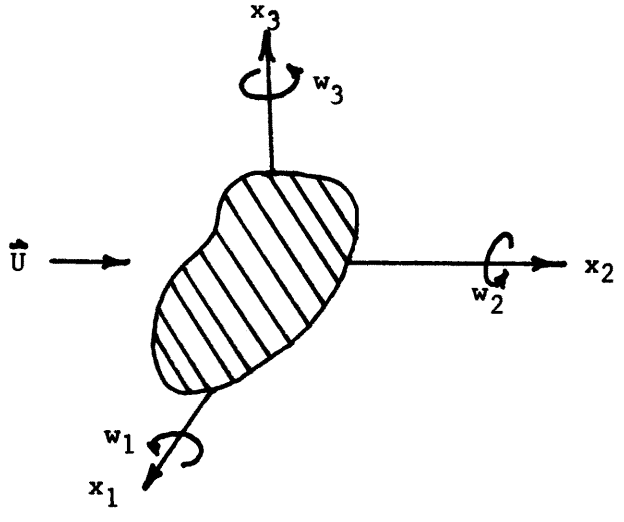

Figure 2.1. Coordinate system and associated rotations.

The velocity which determines the forces and moments acting on the body is the relative velocity $\vec{U}$ between the body and the flow field. Note that the x_2 axis has been chosen to be in the direction of the relative velocity U. The forces acting on the body consist of aerodynamic forces and body forces f_i, and can be described by the following equation:

$$F_i = C_i^n A^n \rho U^2/2 + f_i \qquad (2.1)$$

where F_i, $i = 1,2,3$ denotes the component of the force in the direction of axis x_i, where C_i^n are dimensionless coefficients. The superscript n denotes that the area used in Eq. (2.1) is the projected area on the plane normal to the vector $\vec{U}$. Thus A^n depends upon the orientation of the body with respect to $\vec{U}$. The body forces f_i include gravity forces and possibly additional forces due to large-scale pressure gradients in the field, which can be added to the body forces if the C_i^n are determined for a uniform flow.

It is also possible to express the forces acting on the body in terms of a reference area, A^r which is independent of the orientation of the body:

$$F_i = C_i^r A^r \rho U^2/2 + f_i . \tag{2.2}$$

Moments acting on the body determine the oscillatory or rotational motion. Again one of two formulations can be used, as shown in Eqs. (2.3) and (2.4) to describe the moments acting on a free body,

$$M_i = C_{mi}^n L A^n \rho U^2/2 \tag{2.3}$$

or

$$M_i = C_{mi}^r L A^r \rho U^2/2 \tag{2.4}$$

where L is a typical length.

Certainly the reference area and the normal area formulations are equivalent. One should be aware, however, that the value of corresponding aerodynamic coefficients in the two formulations are quite different. Several authors prefer to use the normal area (A^n) formulation for the following reason. The value of the drag coefficient, $C_2^n = C_D^n$, for various bodies do not vary considerably with the

orientation of the body and can be estimated. The latter formulation using reference areas, on the other hand, is more convenient for describing the average drag on a rotating body, as A^r is constant, independent of the angle of attack θ.

Consider, for example, the body in Fig. 2.2. In position (a) $C_D^n \approx 2$, whereas in position (b) $C_D^n \approx 1$. On the other hand, C_D^r in position (b) is only one-eighth of C_D^r in position (a). This large difference in the second formulation reflects the change in the value of A^n rather than the change in nature of the flow.

This example clearly shows that the main difficulty in estimating the force acting on a free body is in determining its orientation with respect to the flow, rather than in evaluating the exact drag coefficient at a particular known orientation.

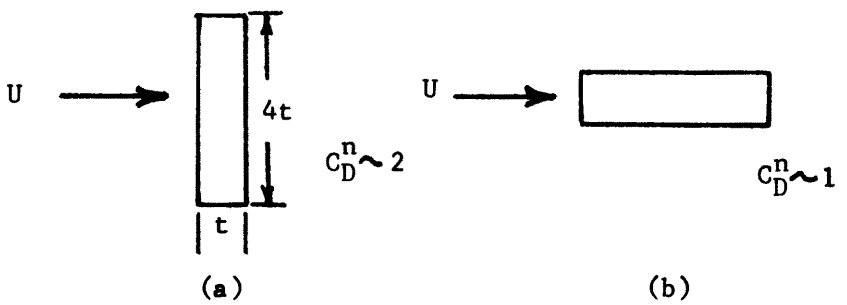

Figure 2.2. Drag coefficients at different orientations for a bluff body.

When the values of the force and moment coefficients for all orientations are known, the motion of a body with six degrees of freedom, can be described by the following differential equations:

$$\frac{W}{g}\frac{dU_i}{dt} = \frac{W}{g}\frac{d^2x_i}{dt^2} = \frac{1}{2}\rho U^2 C_i^r A^r + f_i \qquad (2.5a)$$

$$I_i \frac{dw_i}{dt} = \frac{d^2\theta_i}{dt^2} = \frac{1}{2}\rho U^2 C_{mi}^r A^r L \qquad (2.5b)$$

A similar formulation using the normal area can also be used.

Theoretically, one can examine the motion of a body from given initial conditions in a known velocity field using these equations. In practice, however, the force and moment coefficients, which depend both on the Reynolds number and the rotational speeds, are not known. It is the purpose of the work to examine whether the average motion of a body can be described using simplified formulations.

Motion of Bodies with Large Moments of Inertia

(a) Definition of Dimensionless Parameters

The analysis is largely simplified if one considers a body with a large moment of inertia. The aerodynamic moments created by the flow in this case do not cause a quick response of the body. Thus rapid oscillations or large changes in the rate of rotation are not possible. This is obvious from Eq. (2.5b) which shows that for a relatively large moment of inertia I_i, or relatively small aerodynamic moments, the relative value of dw_i/dt is small.

At this point it is useful to introduce appropriate time scales to describe the flow and the rate of change of the rotational speed of the body. The time scale of the flow, T_f, will be defined as

$$T_f = \frac{L}{U}, \qquad (2.6)$$

where L is a typical length of U is the relative velocity.

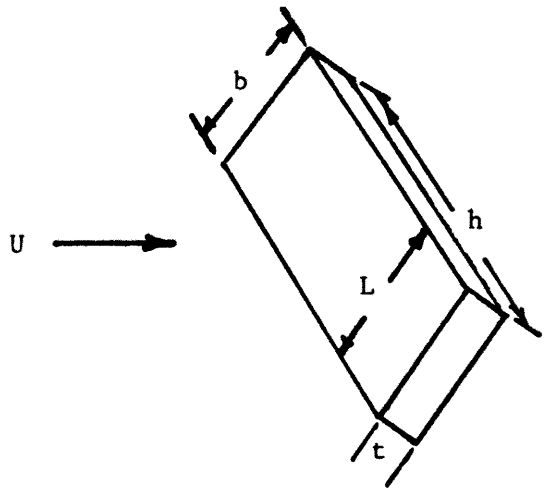

Figure 2.3. Dimensions of elongated rectangular body.

In this work we shall consider elongated rectangular bodies. The length will be described by h, the width by b, and the thickness, which is the smallest dimension, by t, as shown in Fig. 2.3. The time constant, T_f, will be defined using L = b.

The dimensions of the term dw_i/dt are $1/T^2$ and the value of this term defines a time scale,

$$T_w = 1/(dw_i/dt)^{1/2} \tag{2.7}$$

which characterizes the rate of change of the rotation w_i. One is interested in finding when dw_i/dt becomes small compared to $1/T_f^2$, or $T_w >> T_f$. Consider the body shown in Fig. 2.4 and the rotation around the x_3 axis.

Dividing Eq. (2.5b) by $1/T_f^2 = U^2/b^2$, one gets

$$\frac{dw_3}{dt}\left(\frac{b^2}{U^2}\right) = \frac{T_f^2}{T_w^2} = \frac{C_m \rho_a}{2}\frac{A r_L^3}{I_3}. \tag{2.8}$$

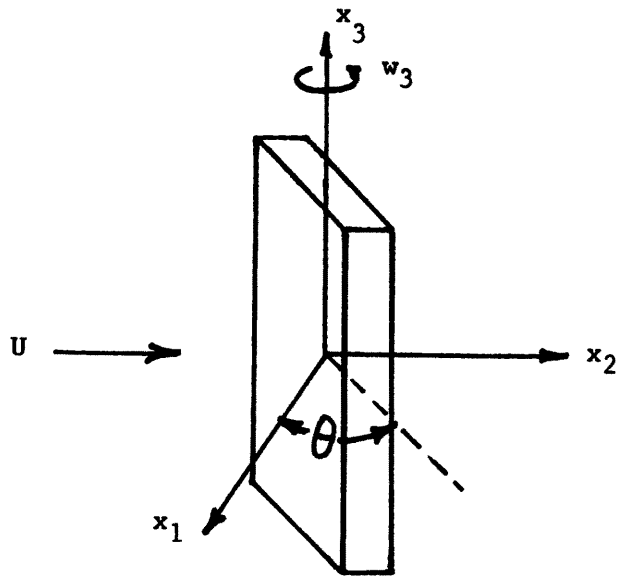

Figure 2.4. Body orientation for the definition of time scales.

Since $A^r = bh$ and $I = \rho_b h b^3 t/12$ on gets from Eq. (2.8)

$$\frac{T_f^2}{T_w^2} = \frac{1}{I''} \tag{2.9}$$

where

$$I'' = \left(\frac{1}{6C_m}\right)\frac{\rho_b t}{\rho_a b} \quad . \tag{2.10}$$

The dimensionless moment of inertia I'' defined in (2.10) depends upon the moment coefficient C_m, and since C_m is a function of the angle of incidence θ, it would be convenient to define a parameter proportional to I'' but independent of θ. Such a dimensionless moment of inertia independent of C_m can be defined as,

$$I^* = \frac{\rho_b}{\rho_a}\frac{t}{b} \tag{2.11}$$

and Eq. (2.9) can be written as

$$\frac{T_w}{T_f} \propto (I^*)^{1/2} \, . \tag{2.12}$$

Similar formulations can be made for $i = 1$ and 2. Note that the body described in Fig. 2.4 will have values of I_1^* and I_2^* larger than that of $I^* = I^*_3$, and thus smaller changes are expected in w_1 and w_2 as compared to w_3. Now, it is clear from Eq. (2.5b) that when the value of I_1^* is increased, the time scale of the corresponding change of rotation is increased. Thus one should expect to find more rapid changes in w_3 than in w_1 and w_2. Similarly in case of a turbulent flow the rms value of w_3 will be larger than that of w_1 and w_2. For this reason in this study only the value of $I^* = I_3^*$ will need to be used.

One has also to define another time scale T_n, associated with the rotation itself, rather than the rate of change of the rotational speed. If the body rotates around an axis at an average rate of n rotations per second, a time scale can be defined as

$$T_n = \frac{1}{n}, \tag{2.13}$$

which is the time it takes the body to make one rotation. It should be noted that T_n can be either large or small, independent of T_w. For example, when $n = 0$, the body could still fluctuate at a high frequency because of a small value of I^*. A dimensionless parameter can be defined as

$$\frac{T_f}{T_n} = \frac{nb}{U}, \tag{2.14}$$

which describes the ratio of the time scales.

We have limited the discussion in this chapter to bodies with large I^* which corresponds to large T_w/T_f. It is useful to further distinguish between three cases:

(a) $\frac{nb}{U} = 0$

(b) $\frac{nb}{U}$ small

and

(c) $\frac{nb}{U}$ large

The first two cases will be considered in this chapter. We shall analyze the case of large nb/U in Chapter 3.

(b) The Case of nb/U = 0

Consider a body oriented in the flow so that $M_i = 0$ and $w_i = 0$. Obviously the problem is simplified as one needs to consider only the translatory motion of the body. It is necessary to examine, however, if such an orientation would be stable for small perturbations as well as for large perturbations. Of particular interest is the determination of whether such an orientation is stable for the perturbations generated by the flow around the body.

Previous studies and observations clearly indicate that flat bodies oriented with their large surface normal to the flow are stable for small perturbations.

Willmarth [8] has studied the aerodynamics of oscillating discs. The discs were found to oscillate when oriented with their faces normal to the flow. His experiments showed that the measured frequency of oscillation satisfied the equation

$$\frac{\omega b}{U} = (I^*)^{-.44} \tag{2.15}$$

where I^* is a dimensionless moment of inertia defined in his case as $I^* = I/\rho_a d^5$, where d is the diameter of the disk and I its moment of intertia. The similarity to Eq. (2.12) is obvious. Willmarth

has also found that $dM/d\theta < 0$, for values of θ up to 10° (where M is the restoring moment acting on the body and θ is an angle of incidence to the flow defined so that at $\theta = 0$ the body is oriented with its large face towards the flow). This finding indicates that the position $\theta = 0$ is basically stable for quite large perturbations.

The stability of this orientation for large perturbations would depend on the magnitude and frequency of the perturbations. Consider, for example, perturbations that are generated by the flow itself, like vortex shedding. Their frequency is inversely proportional to the time scale of flow. Obviously, if T_f is much smaller than T_w, the characteristic time of change of rotational speed, the body would not be able to respond and would remain stable. Since small values of T_f/T_w correspond to large values of I^*, as indicated by Eq. (2.12), it is concluded that bodies with large dimensionless moments of inertia would be stable and would not rotate due to the effect of their self-generated disturbances. As it will be shown later this conclusion has been confirmed experimentally for a wood plank with $I^* = 200$. On the other hand, experiments show that strips of paper falling in air which have $I^* < 10$ are not very stable and easily enter a rotational mode.

It is impossible to determine whether such a translatory motion would be stable in a typical tornado field which is highly nonuniform, has large vorticity, might have large velocity fluctuations and where the initial conditions might include some rotation. One has, therefore, to assume that this mode of motion, where $n = 0$, will be stable in some tornado generated missiles which usually have a large value of I^*, but unstable in others.

When such a position is stable, the drag coefficient C_D^n would be of the order of 2 and the translatory motion could be readily estimated using Eq. 2.5a.

From the previous discussion it is clear why in the case of elongated bodies, rotation induced by the fluctuating forces will usually occur around the long axis of the body, namely the x_3 axis, where $I^* = I_3$ has the smallest value. It is also noted that the moments acting on an elongated body around the other axes are relatively smaller. Consider for example the two bodies described in Figs. 2.5a and 2.5b,

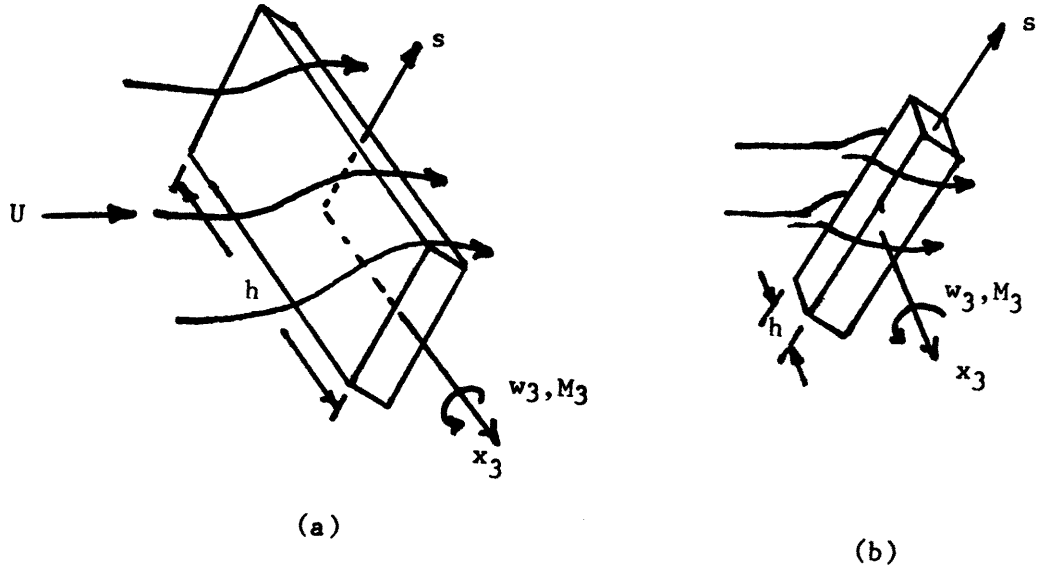

Figure 2.5. Flow around bodies of differing length dimension h.

which differ only in their x_3 dimension. The moment per unit length (M_3/h) in case (a) is expected to be larger than in case (b), since the variation of the flow in the direction of axis s is smaller in

case (b). Thus the body in case (b) is more likely to rotate around the axis s where the I_s^* value is smaller, and not around the x_3 axis where both I_3^* is large and M_3 is small.

(c) The Case of Small nb/U

When considering a body which steadily rotates slowly relative to the flow (nb/U small), it may be assumed that the aerodynamic coefficients at each instant of time (or angle θ), could be approximated by the "static" coefficients of a stationary body at the corresponding angle of incidence. This approximation is called the quasi-static approximation. Thus, if one considers a symmetric body rotating at a small nb/U, its average lift force over a complete rotation is zero.

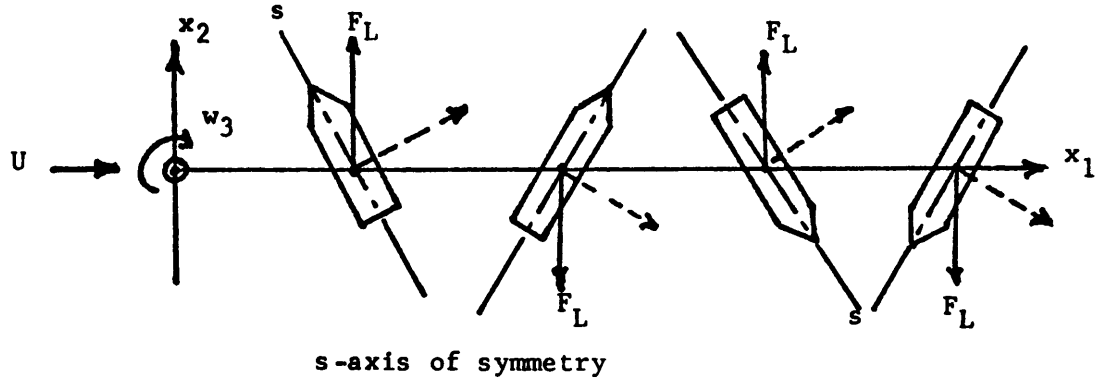

Figure 2.6. Lift forces acting on symmetric body during rotation.

One can also conclude that during translation in the x_1 direction, the average motion in the x_2 direction is zero. Thus, if one assumes very small steady rotational rates, it is possible to neglect the effect of the lift and to describe the average motion of the body by a motion of a material point which is acted on by a drag force.

Even though the drag will be a function of time one could define an average drag coefficient in the x_2 direction. If a body has large I^*, its mass would usually be large and the velocity U would hardly change during one rotation. Thus, the average force can be calculated assuming a steady rotational speed and constant U, so that

$$\overline{F}_D = \frac{1}{2\pi} \int_0^{2\pi} C_D^r(\theta) \frac{\rho U^2}{2} A^r \, d\theta = \frac{1}{4\pi} \rho U^2 A^r \int_0^{2\pi} C_D^r(\theta) \, d\theta .$$

Defining an average drag coefficient as

$$\overline{C}_D = \frac{1}{2\pi} \int_0^{2\pi} C_D^r \, d\theta , \tag{2.16}$$

one can write that

$$\overline{F}_D = \frac{1}{2} \rho \overline{C}_D U^2 A^r .$$

Modi and El-Sherbiny [2] presented measurements of C_D^r of a flat plate as a function of the angle θ, as shown in Fig. 2.7 (A^r is the area of the plate).

Using such data, $\overline{C}_D$ for small nb/U can be calculated. Our calculations for the above data show that $\overline{C}_D \simeq 1.05$. If the effect of blockage in the these experiments is taken into consideration a slightly smaller value $\overline{C}_D \sim 1.0$ is found.

Following Smith [6] a similar expression can be derived for the average moment coefficient $\overline{C}_m$ where

$$\overline{C}_m = \frac{1}{2\pi} \int_0^{2\pi} C_m(\theta) \, d\theta \tag{2.17}$$

which would indicate whether the rotational speed will increase or decrease. Obviously for symmetric bodies $\overline{C}_m$ is zero and therefore

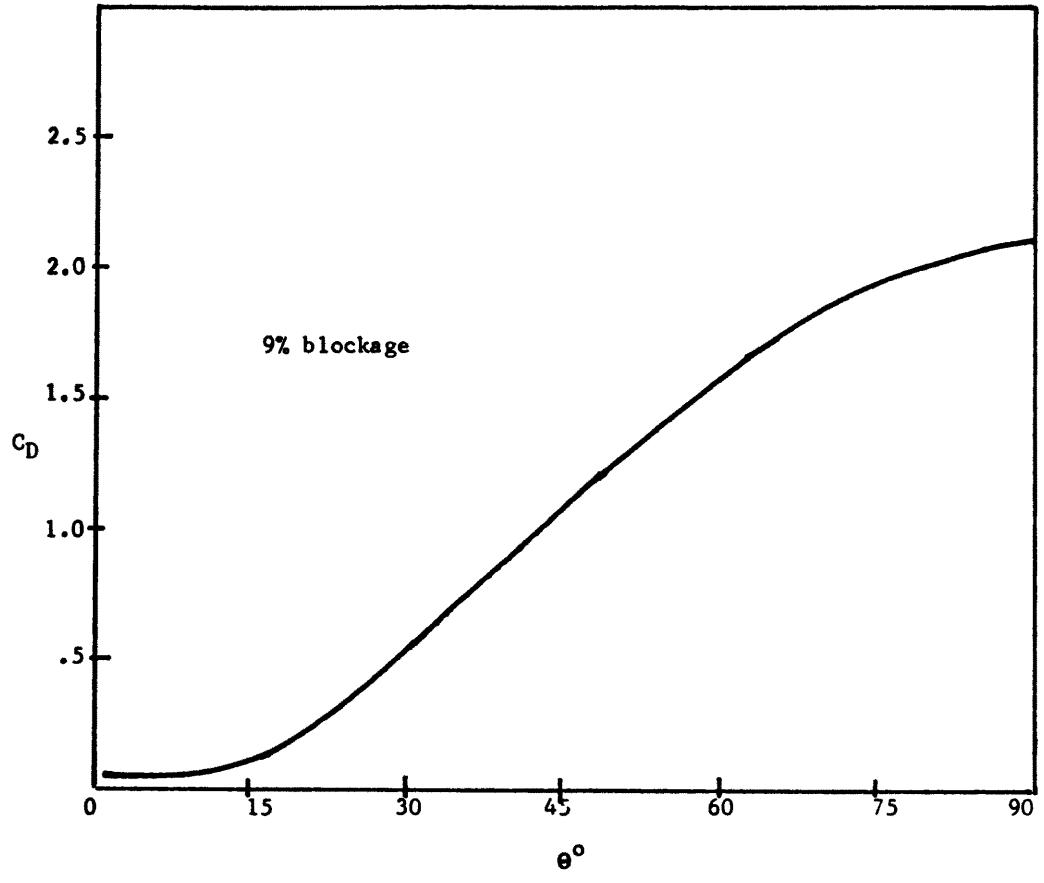

Figure 2.7. Typical drag coefficients of a flat plate at different angles of attack.

one would expect a steady rotational motion. However, this conclusion would not be correct if the rotational motion affects the aerodynamics of the flow. This case corresponds to the category of large nb/U, but it is not clear what value of nb/U can be considered to be large. Smith considered the problem and came to the conclusion that the translational motion could easily induce either a small positive or negative $\overline{C}_m$ at small values of nb/U, which is not obvious from the consideration of the static moments.

If the body is not symmetrical and particularly if the center of gravity does not coincide with the center of pressure, rotation can be easily induced. Smith presented tests with a nonsymmetrical nose cone whose cross section (normal to the x_3 axis) is circular with centers of gravity at different locations along the x_3 axis. The results of this study showed that when the center of gravity was placed midway along the length of the body no rotation occurred around the x_2 or x_1 axes. Due to the symmetrical cross section, no rotation would be expected about x_3, the long axis of the body. Changing of the position of the center of gravity, from the midpoint along the long axis, did induce rotation about the nose cone's smaller axes. In these cases the value of the average drag coefficient was quite close to value found by applying Eq. (2.17).

Thus, one may conclude that when nb/U is small, it is possible to consider only the translatory motion of the center of gravity of the body using an average drag coefficient estimated from the quasi-static approximation.

Chapter 3

AERODYNAMICS OF AUTOROTATING BODIES

In the previous chapter the significance of the dimensionless parameter nb/U to the dynamics of the motion of rotating bodies was discussed. When nb/U is small, the forces acting on such a body can be evaluated using the quasi-static approximation. However, when nb/U becomes large, the rotation induces significant circulation around the body. The circulation modifies the flow field and changes the forces acting on it. In particular, a circulation dependent lift force due to a Magnus effect is expected to occur. Now, observations suggest that a steady state rotation around the longitudinal axis may exist for many types of elongated bluff bodies. Namely there is a certain value of n_3 for these bodies such that $n_3 \neq 0$ and $dn_3/dt = 0$. This type of motion will be classified as <u>autorotation</u> (see Fig. 3.1a). Several authors use instead the term "tumbling," which will be used to describe such a motion. In this work the term tumbling will be used to describe motion with appreciable rotation around more than one axis, as shown in Fig. 3.1b.

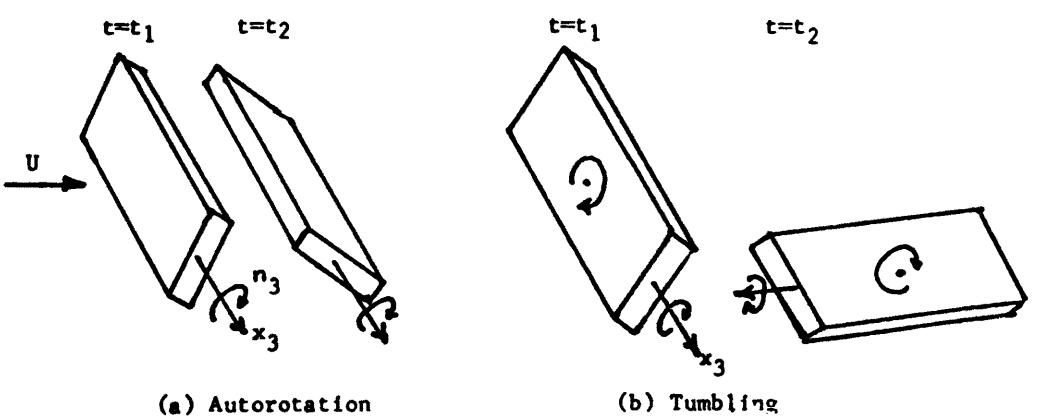

Figure 3.1. Body motion during autorotation and tumbling.

In this chapter an analysis will be made of the autorotational mode in order to find: (1) What is the value of nb/U for which a steady autorotation will be sustained by a relative velocity U of the fluid with respect to the body and how does it depend on the relative dimensions of the body. (2) What are the lift and drag forces acting on such steady autorotating bodies.

The Value of nb/U in Steady Autorotation

We shall limit the discussion to elongated bluff bodies with a rectangular cross section as described in Fig. 3.2.

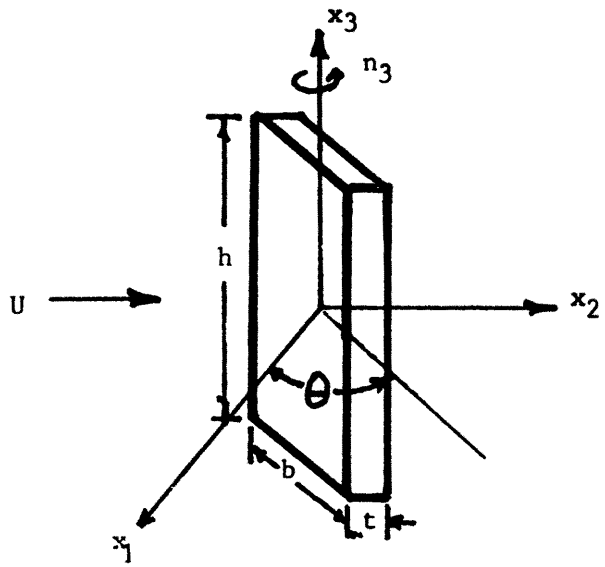

Fig. 3.2. Orientation of body during autorotation.

The body is assumed to rotate only aroung the x_3 axis. We saw earlier that the dimensionless moment of inertia I_3^* was the smallest, and that observations indicate that autorotation will usually occur around this axis.

The value of n denotes the number of rotations per second. It should be stressed that the instantaneous angular velocity of the body,

w_3 , need not be constant. If $I_3 = I^*$ is not large, it is quite possible that quasi-steady rotation will exist in which $dw/dt \neq 0$ and $w = \bar{w}(1 + f(\theta))$. In this equation f is a periodic function of θ , namely $f(\theta + 2\pi) = f(\theta)$ or $f(t + T) = f(t)$ where the period $T = 1/n$, in this case related to w by

$$n = \frac{1}{2\pi}\left[\frac{1}{T}\int_0^T w dt\right] = \frac{\bar{w}}{2\pi} .$$

The value of n depends on the geometry of the cross section, the length of the body, its moment of inertia I_3 , the relative velocity U and the properties of the fluid. Using dimensional analysis one finds that in steady state,

$$nb/U = F(I^*, k, Re, t/b) , \qquad (3.1)$$

where $k = h/b$. (Appendix II gives an analysis for Eq. 3.1.)

Since by definition $t \leq b$, the maximum value of t/b one should consider is one. In the case of flat bodies, its value can be much smaller than one, and at the limit, when t/b is small, nb/U should be independent of the ratio t/b. On the other hand, as t/b approaches one, the cross section will be more symmetrical and the value of nb/U will probably be reduced. Most of the available data are for small t/b. We shall assume that for these data, nb/U is not a function of t/b. Later we shall see that the effect of increasing t/b up to $t/b = 1/3$ is not very large.

The effect of the Reynolds number on the rotation of bluff bodies is expected to vanish at large values which usually exist in auto-rotating tornado generated missiles. Therefore, we assume that $nb/U \neq f(Re)$ and thus it is possible to write that

$$nb/U = f(k, I^*). \qquad (3.2)$$

Let us consider now the limits of Eq. 3.2 for large value of k and I^*. The role of k in this equation is to describe the edge effects. Thus, as $k \to \infty$, namely when the body is very long, one would expect most of the flow to be two-dimensional $(d/dx_3 = 0)$. In this case, nb/U would be independent of k. From previous experience this limit would be reached when $k = h/b > 20$. On the other hand when k becomes smaller, the flow around the edges would reduce the Magnus Effect and decrease the value of n. This point was discussed in Chapter 2, (see Fig. 2.5). Thus one may conclude that the effect of k would be recognized only for $k < 20$ and the effect would be to decrease the value of nb/U.

Consider now the effect of the dimensionless moment of inertia I^* on the motion. If I^* is small, dw/dt might be significant and $w(t)$ within one cycle will change considerably. However, when I^* becomes large, the body is not going to respond to relatively high frequency fluctuations of the moments induced by the flow. Recall that I^* gives the ratio of the characteristic time of the rate of change of w to the time constant of the flow. Therefore, for large I^*, one would expect to find $w(t) = 2\pi n = \text{constant}$. At this stage the flow will be determined by the steady rotational motion of the boundary of the body and there is no way in which the density of the body can affect the flow. Since $I^* = \rho_b t/\rho_a b$, one deduces that when I^* becomes large, the value I^* will not affect the value of nb/U.

Therefore, one may conclude that for a large Reynolds number, $k > 20$, and small t/b, an asymptotic constant value independent of these variables exists.

$$\frac{nb}{U} = \frac{nb}{U}\bigg|_{as} = \text{constant}.$$

It is difficult to evaluate theoretically the asymptotic value of nb/U. However it is reasonable to expect that the tangential velocity U_t of the tip of the body would not be much larger than U. When $U_t = \pi b \cdot n = U$, it follows that

$$nb/U = \frac{1}{n}$$

or

$$\frac{U}{nb} \simeq \pi \ .$$

Thus in the asymptotic case one would expect to have $U/nb\big|_{as} \geq 2$. It should be stressed that the above conclusions do not imply that a body with a large value of I^* will easily enter an autorotational mode. In fact since such a body would not respond to the fluctuating forces due to the vortex shedding, it is expected that autorotation would have to be started by a large disturbance other than the disturbances generated by the flow around the body.

Analysis of Dupleich's Data

Dupleich [1] has studied the motion of elongated rectangular bodies falling down due to gravity. In most of his experiments, thin strips of paper were used with $I_3^* = 0(1)$ and $t/b << 1$. In some of his experiments rectangular slats of lead and iron were dropped in water. Since the ρ_a in Eq. 2.9 in the water tests corresponds to the density of water, the values of I^* were about the same as in the experiments with paper strips falling in air. The value of t/b in the water experiments were as large as 0.3. Unfortunately, the maximum value of k in Dupleich's experiments was 8. Moreover, the Reynolds number was not very large. In addition it is not absolutely certain that a steady state autorotation had been reached in some of the experiments.

Dupleich's analysis of the data is different from ours and he did not attempt to express the dependence of U/nb as a function of the above dimensionless parameters. Instead, he used the loading factor Δ, (weight/unit area), as a dependent parameter. Dupleich did not calculate the values of C_D and C_L corresponding to his data either.

Using the given values for t/b of his data (see Table 1, Appendix I), one can correlate the loading factor Δ with I^* as follows. Since Δ is the weight per unit area of the body, the density of the body ρ_b can be written as

$$\rho_b = \frac{\Delta(b)(h)}{g(b)(h)(t)} = \frac{\Delta}{gt} \quad ,$$

where g is the acceleration due to gravity. Therefore, the dimensionless moment of inertia about its longitudinal axis using Dupleich's data is given by

$$I^* = \frac{\rho_b t}{\rho_a b} = \frac{\Delta t}{gt\rho_a b} = \frac{\Delta}{\gamma_a b} \quad ,$$

where γ_a is the specific weight of the fluid.

Using this procedure, the values of U/nb and I^* for all his experiments were calculated and are presented in Appendix I. Only one set of tests, with cigarette paper, has not been analyzed as it was noted by Dupleich that the stiffness of the paper strips was not sufficient, and bending occurred along the x_3 axis.

Dupleich also measured the angle of descent of the falling bodies. Using his measurements, the value of $\overline{C}_D$ and $\overline{C}_L$ acting on the body can be calculated. Figure 3.3 shows an autorotating body in two dimensions with the longitudinal axis into the paper. The body is descending at an angle α with respect to the ground, and the relative velocity is shown as U. The vectorial sum of the lift and drag acting

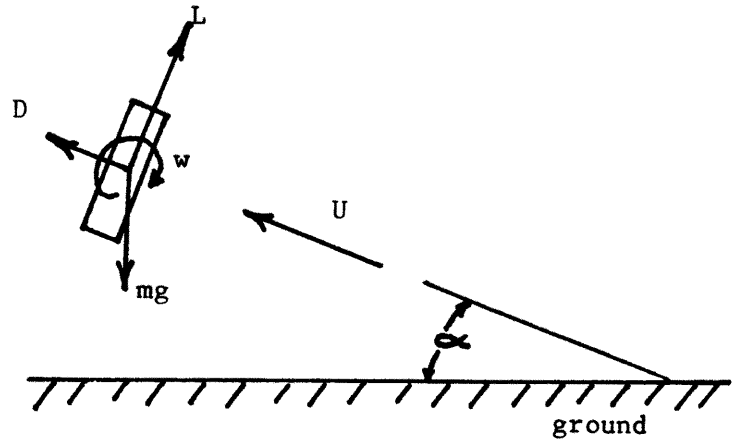

Figure 3.3. Descent of autorotating body.

on the body is equal to the weight of the body, mg. Thus the drag force $D = mg\sin\alpha$. Now $mg = \Delta \cdot A^r$, where $A^r = b \cdot h$ is the reference area. Thus one finds that

$$\overline{C}_D = \frac{D}{\frac{1}{2}\rho_a U^2 A^r} = \frac{2\Delta\sin\alpha}{\rho_a U^2} \tag{3.3}$$

and

$$\overline{C}_L = \overline{C}_D/\tan\alpha \tag{3.4}$$

Using Eqs. 3.3 and 3.4 the drag and lift coefficients for Dupleich's data were calculated and are presented in Appendix I.

Discussion of the Experimental Results

The dependence of the dimensionless parameter U/nb on the aspect ratio $k = h/b$ is shown in Fig. 3.4 for several values of I^*. The data confirms that U/nb for each value of I^* is a monotonically

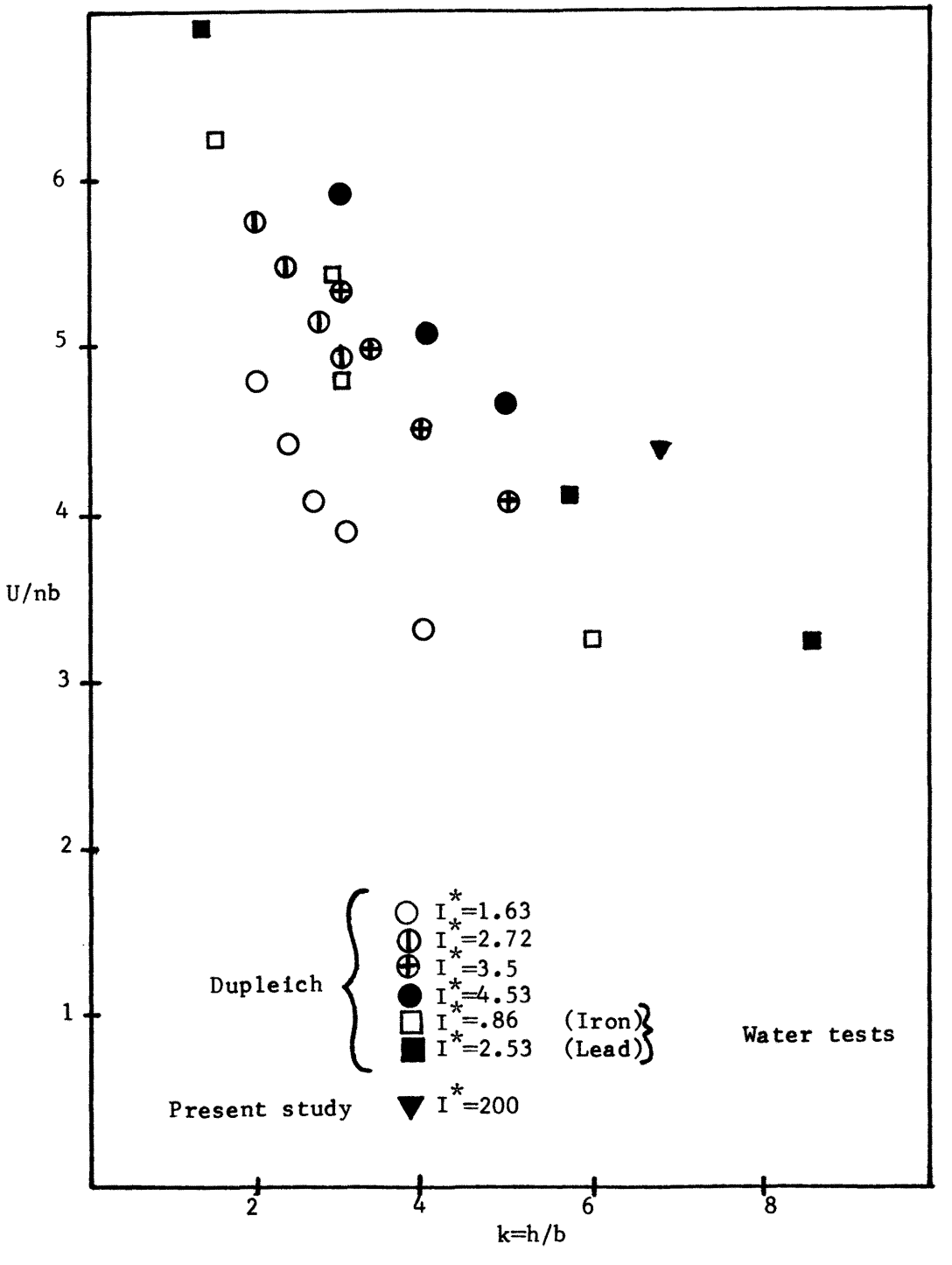

Figure 3.4. Dependence of U/nb on aspect ratio k for an autorotating body.

decreasing function of k, namely a slower rotation exists for small values of k. Unfortunately, most of the data are for $k \leq 4$ and the maximum value of k in Dupleich's study was $k \sim 9$, for which one still expects to find a significant edge effect. Thus, it is impossible to determine from this figure the exact value of $U/nb\big|_{as}$, which appears to be around 2.

The increased value of U/nb at small values of k is consistent in that significant autorotation occurs around the longitudinal axis, x_3 in our notation. Note that the ratio I^*_3/I^*_2 is inversely proportional to k. When $k = 1$, $I^*_3 = I^*_2$, and complete symmetry with respect to these axes exists. When k is smaller than 1, namely h/b is further decreased so that h is smaller than b, the edge effects will cancel the moments which would maintain rotation around the x_3 axis while the rotation around the x_2 axis, which now becomes the longitudinal axis, will be significant.

The effect of I^* on U/nb is shown in Fig. 3.5. It seems as though U/nb increases initially with I^*, but later reaches a maximum. However, the values of I^* did not sufficiently vary in Dupleich's tests to confirm that as I^* becomes large U/nb is independent of I^*. A test, which will be described in Chapter 4, was made during this study with a large model having $I^* \sim 200$. A value of $U/nb = 4.4$ (see Fig. 3.5) was measured in this test. This result supports the previous conclusion that an asymptotic value of U/nb does exist for $I^* \to \infty$. Of course this value is a function of k.

The values of the drag coefficient C_D calculated from Dupleich's data are plotted in Fig. 3.6 as a function of k and in Fig. 3.7 as a function of I^*. It is apparent from Fig. 3.6 that k does not affect

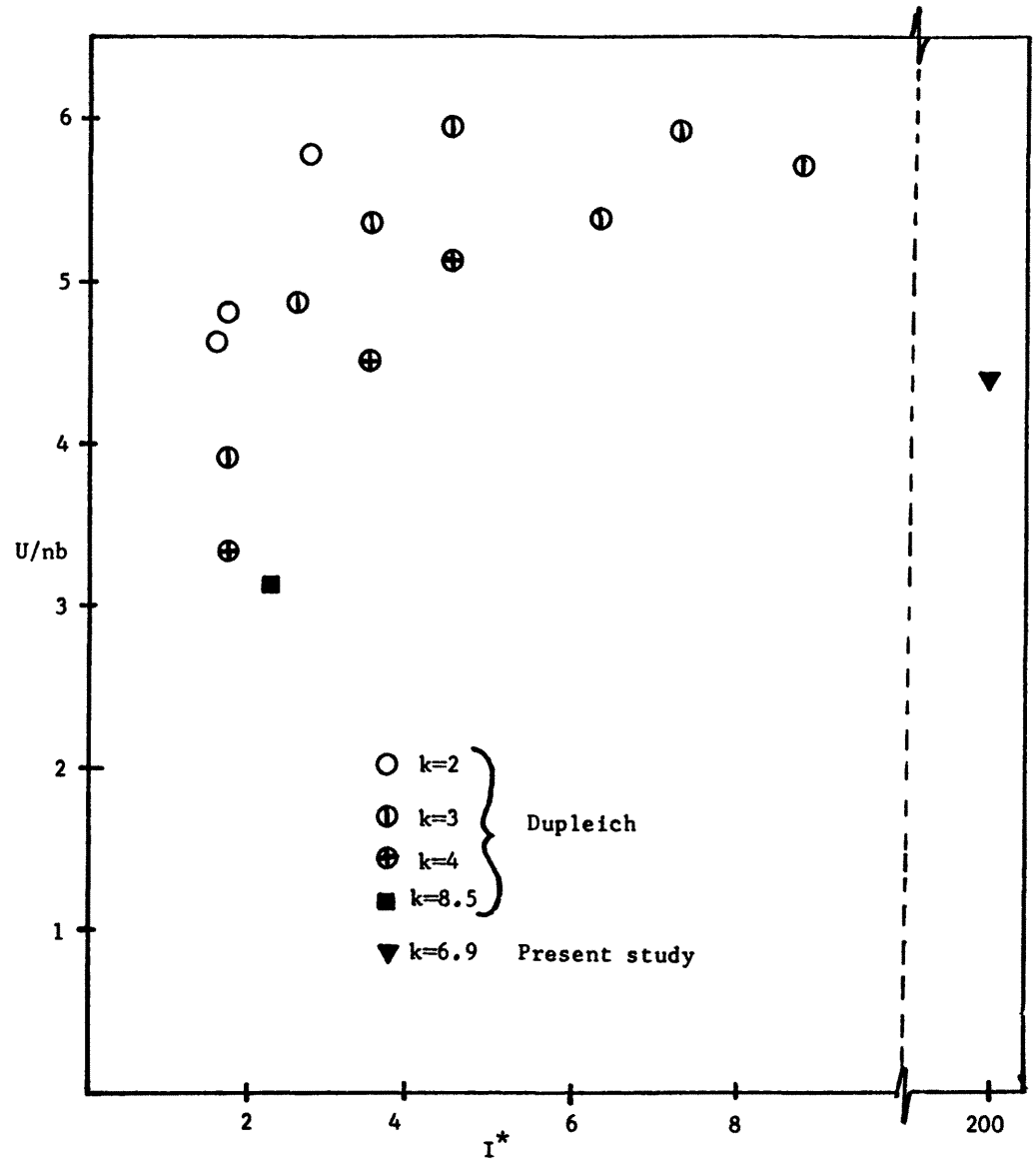

Figure 3.5. Dependence of U/nb on dimensionless moment of inertia I* for autorotating body.

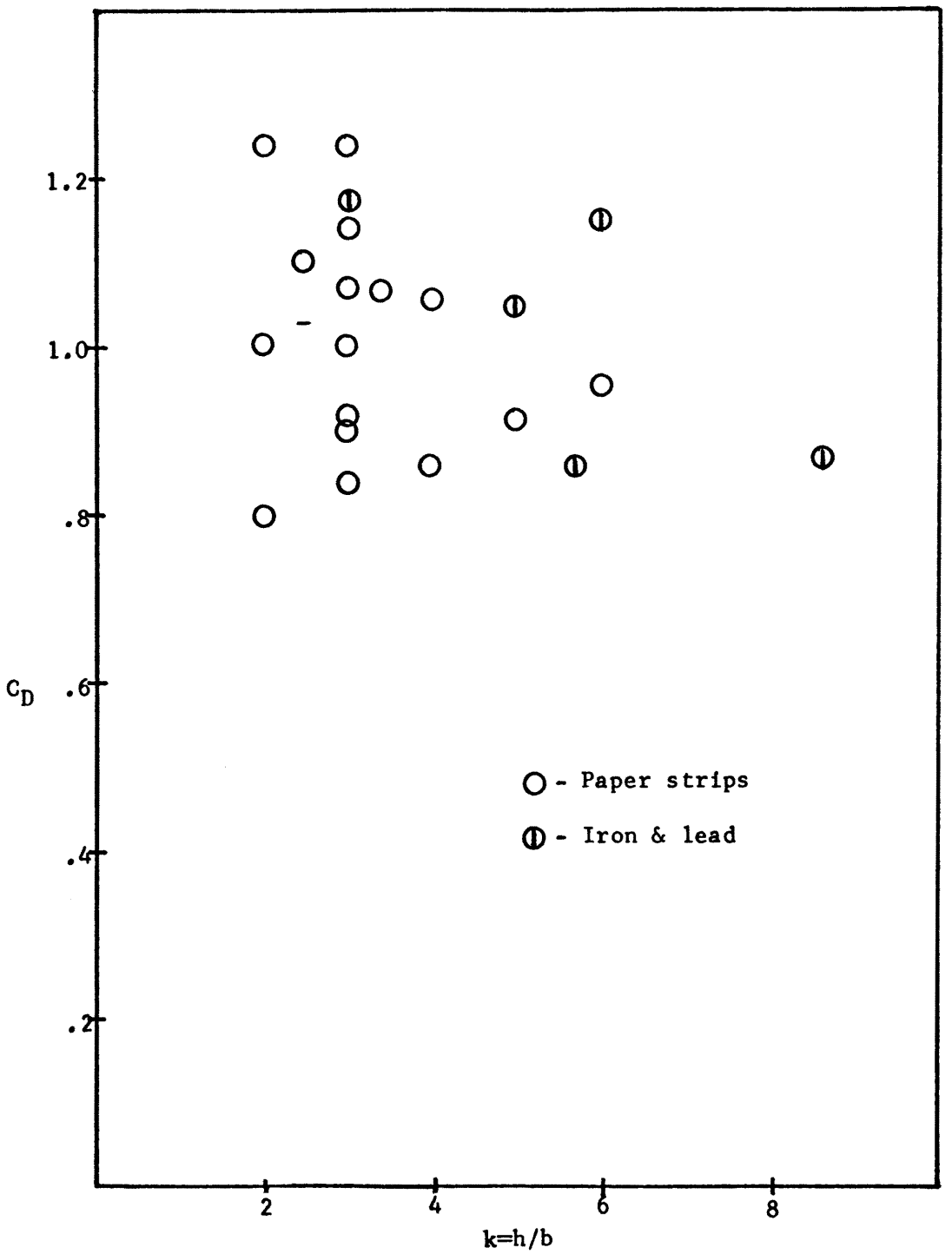

Figure 3.6. Drag coefficient versus aspect ratio k.

the drag coefficient as much as it affects the rotation of the body. Figure 3.7 on the other hand shows a more coherent dependence of C_D on I^*. The figure suggests that C_D is a function of I^* only when I^* is smaller than 10, probably because $w(t)$ is not constant in this range. When I^* is larger than ten, a constant value of $C_D \tilde{} 0.8$ is found for all the experiments with paper strips. Now it will be recalled that (Fig. 2.7), we have estimated earlier using the data of Modi, et al. and the quasi-static approximation that $\overline{C}_D$ for flat bodies should be around 1.0. These two values seem to be close and it appears that the quasi-static approximation can be used for roughly estimating the drag of bodies even at large values of nb/U.

The dependence of C_L on I^* is shown in Fig. 3.8. No clear relationship between these two parameters is evident. On the other hand it appears from Fig. 3.9 that C_L is related to k. Since the lift is mainly a function of the circulation induced by the rotation, it was decided to examine the relationship between C_L and U/nb, which was plotted in Fig. 3.10. It is evident from this figure that C_L is indeed primarily a function of U/nb. The lift coefficient measured in the present study, see Chapter 4, with $I^* \sim 200$, shown in the figure as a triangle, also supports this conclusion. One must note that the data in this graph cannot be extrapolated toward $U/nb = 0$, because the minimum value of U/nb for $k \to \infty$ is expected to be around 2.

We have also examined whether a similar dependence of C_D on U/nb can be established. It is clear from Fig. 3.11 that such a dependence does exist.

Note that in Fig. 3.11 the two values of C_D measured in the present study with $I^* \tilde{} 200$, which are around $\overline{C}_D \tilde{} 1.75$, are shown.

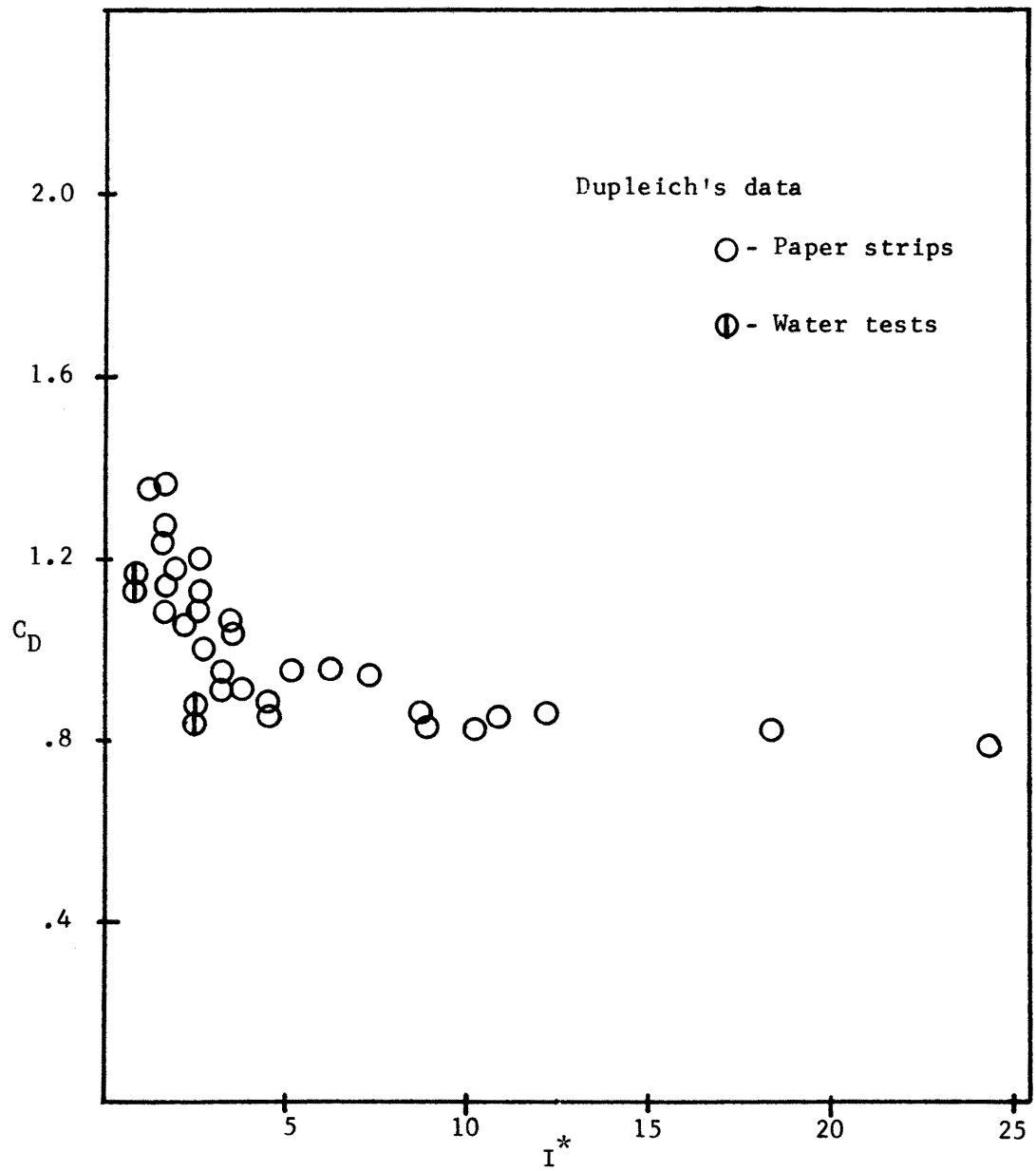

Figure 3.7. Dependence of drag coefficient on dimensionless moment of inertia I^*.

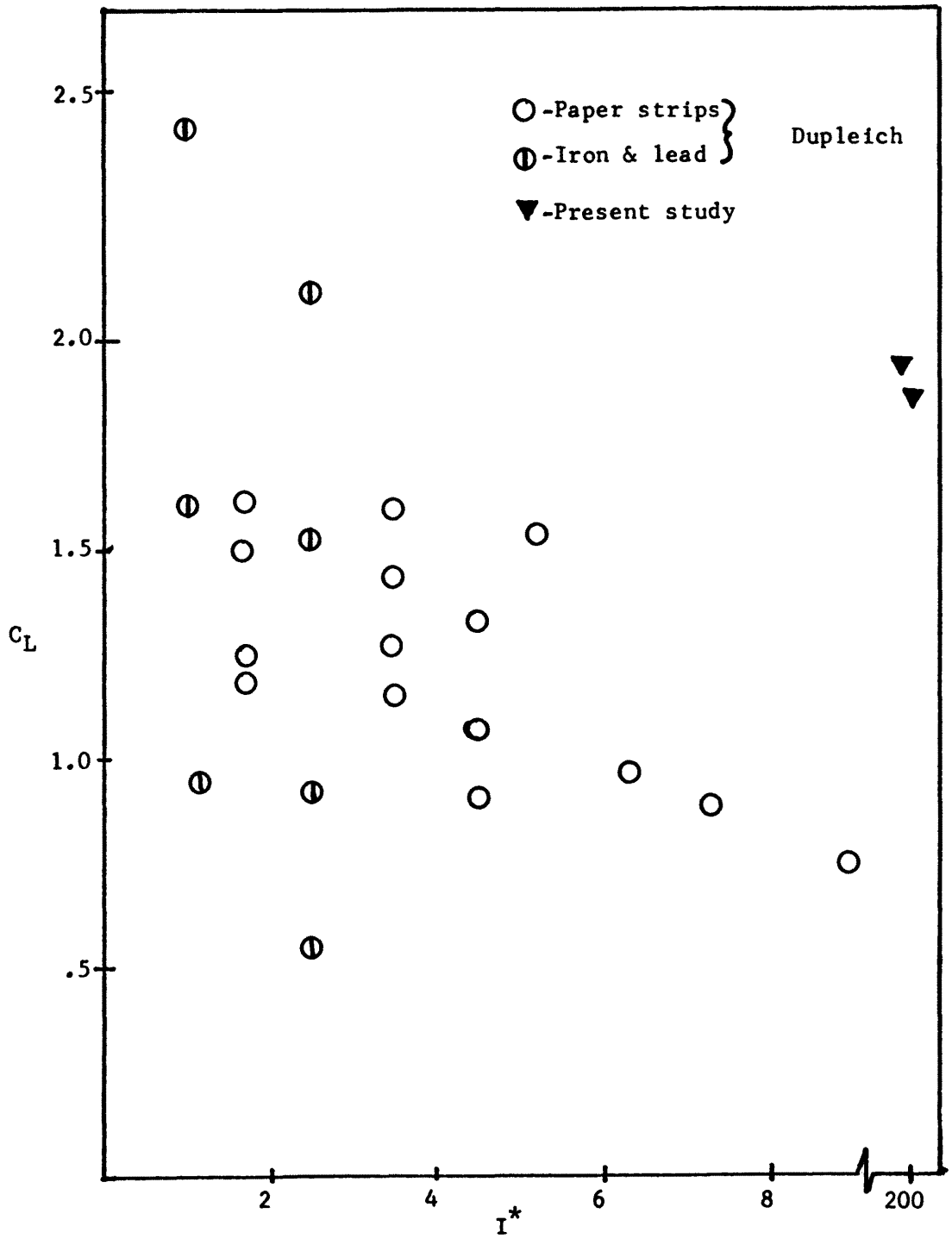

Figure 3.8. Dependence of lift coefficient on the dimensionless moment of inertia I*.

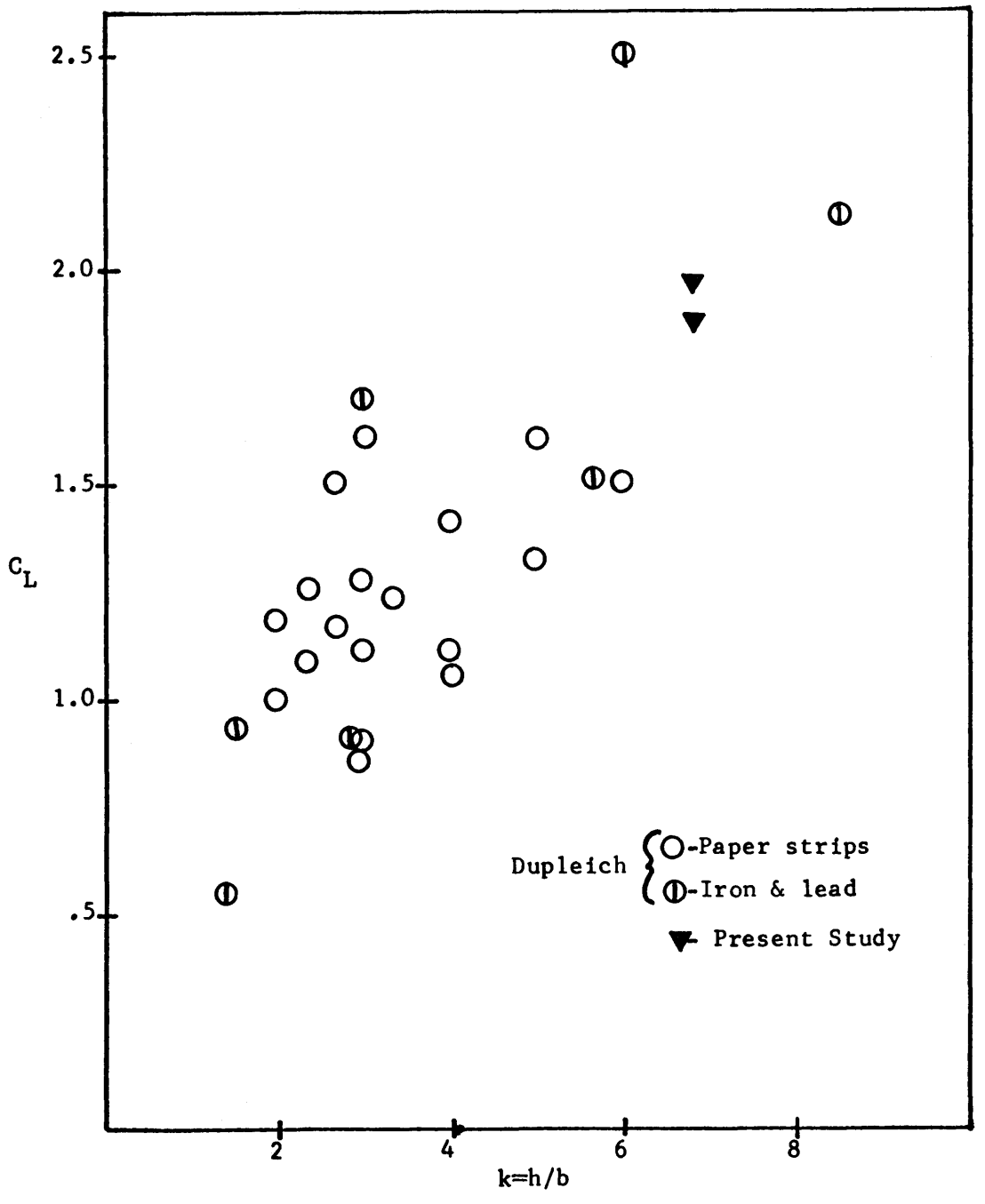

Figure 3.9. Dependence of lift coefficient on the aspect ratio k.

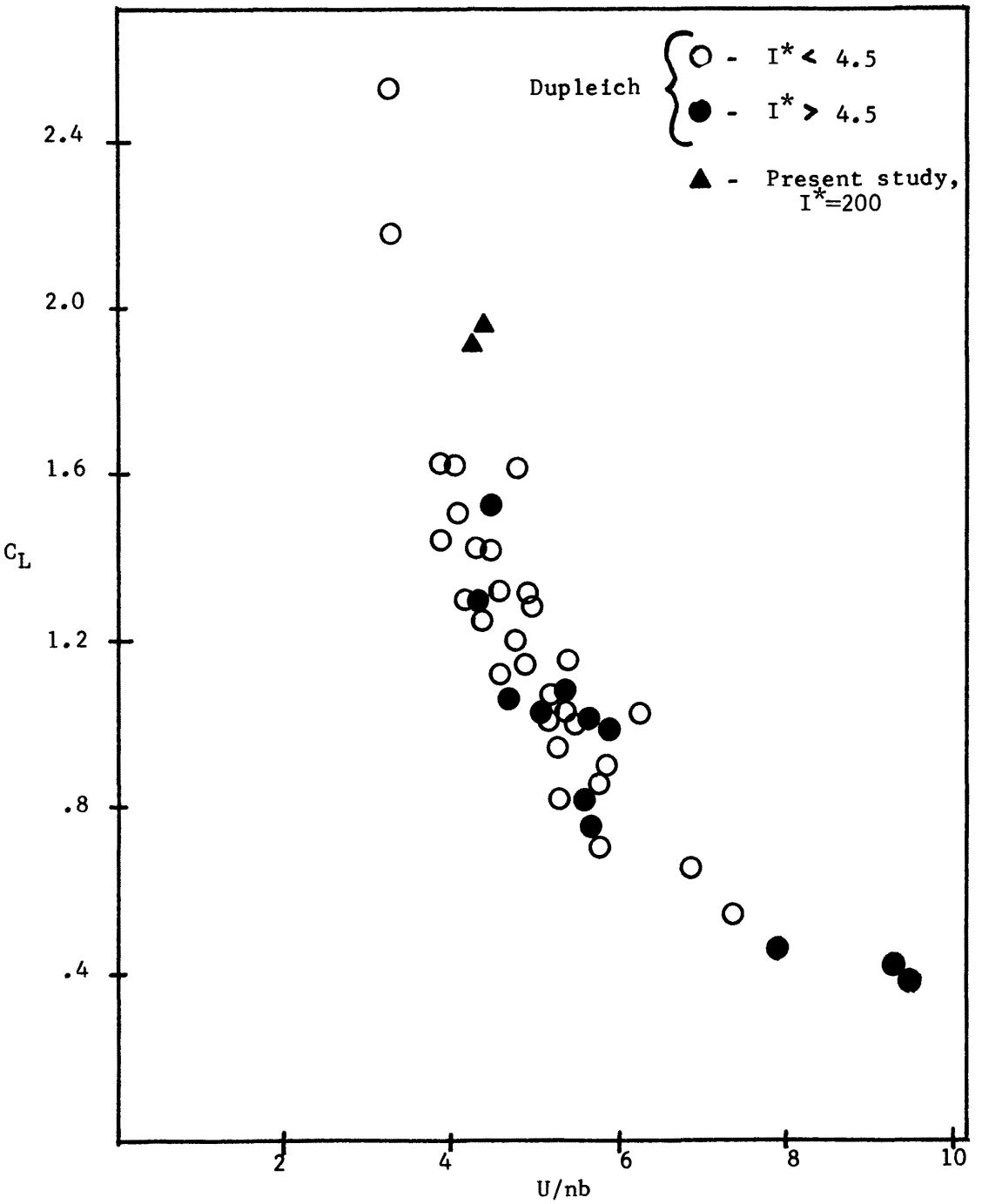

Figure 3.10. Dependence of lift coefficient on the rotational parameter U/nb.

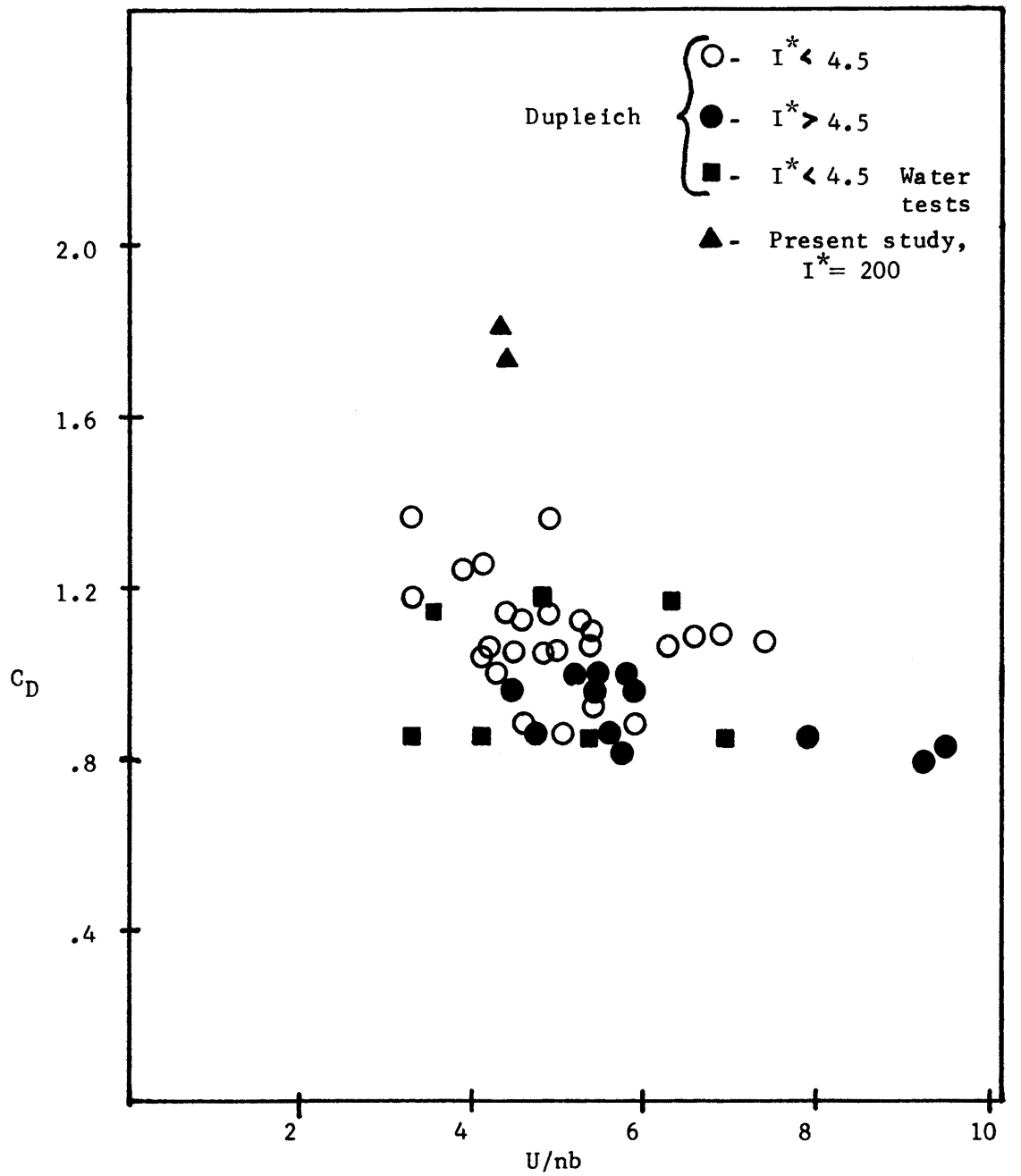

Figure 3.11. Dependence of drag coefficient on the rotational parameter U/nb.

Now t/b in this case was 1/3 and for such a ratio the quasi-static approximation gives an estimated value of $\overline{C}_D \tilde{} 1.5$. It should also be recalled that the Reynolds number of the flow in this case was about two orders of magnitude larger than in Dupleich's experiments and that no correction of blockage has been applied to the wind tunnel data. This explains the difference in C_D between the data of Dupleich and this experiment, and confirms the previous conclusion that the quasi-static approximation can also be used to roughly estimate the drag of auto-rotating bodies.

Chapter 4

A WIND TUNNEL MODEL OF AN AUTOROTATING BODY

During the course of this study, limited experimental program aimed at modeling some tornado generated missiles was carried out. The experimental work can be separated into two parts: tests of an autorotating body whose purpose was to extend Dupleich's data to cases of autorotating bodies with a large moment of inertia, I*, and; measurements of drag coefficients of a static, large bluff body. The measurements in the latter part are not related directly to the main course of the investigation and were therefore presented to the sponsor in a different form.

Test of Autorotating Body

The experimental work was performed in the Meteorological Wind Tunnel of the Fluid Mechanics and Wind Engineering Program at Colorado State University. The tunnel has a nominal cross section of six by six feet in which a model of an autorotating body was installed. The tunnel is a closed circuit facility with variable wind velocities from 1 to 90 feet per second. An overview of the tunnel is shown in Fig. 4.1.

In order to simulate autorotation of a bluff body with large I*, a rectangular body made of wood, as shown in Fig. 4.2a, was constructed. The body was mounted on a one inch shaft with precision bearings as shown in Fig. 4.2b. The mounting allowed the body to rotate around the shaft with very little friction. The shaft was connected to the ceiling of the tunnel with a universal joint (point A in Fig. 4.2a), which allowed the shaft and the body to deflect

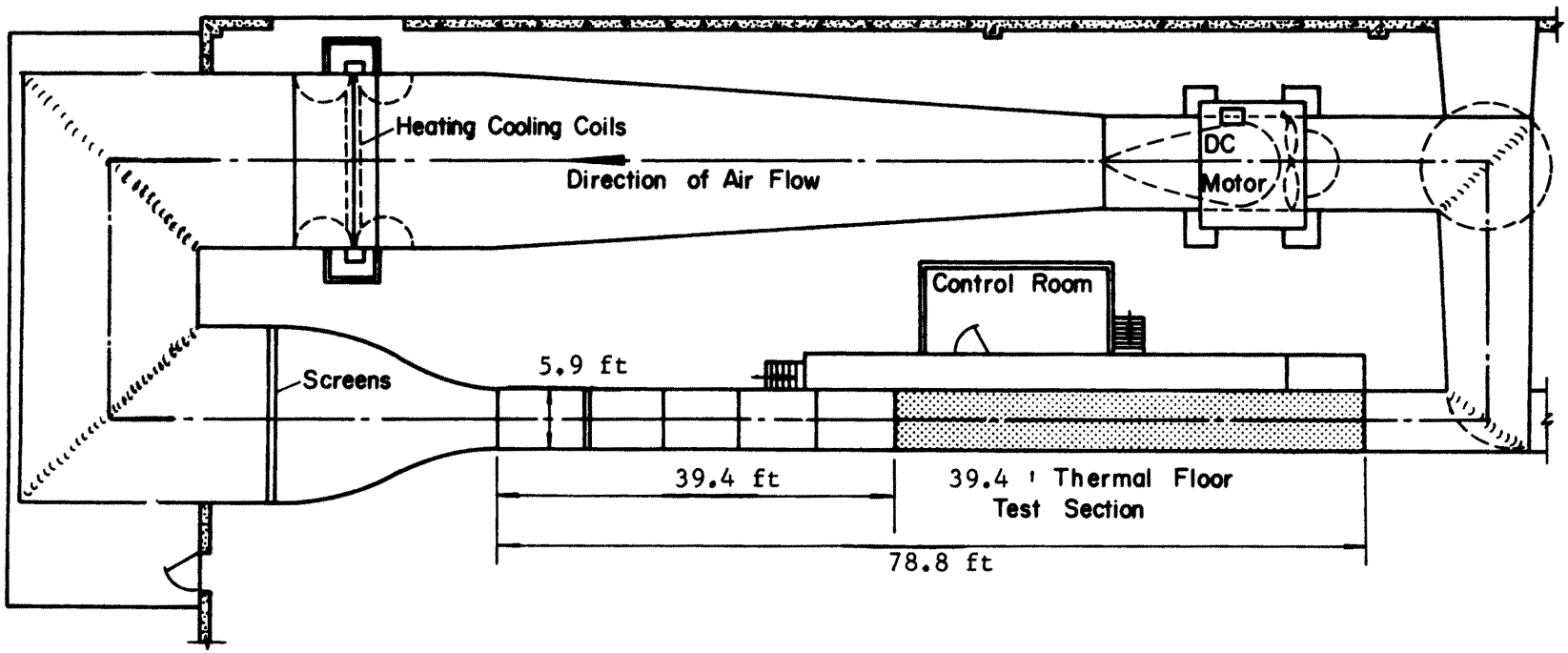

Figure 4.1. Colorado State University Meteorological Wind Tunnel.

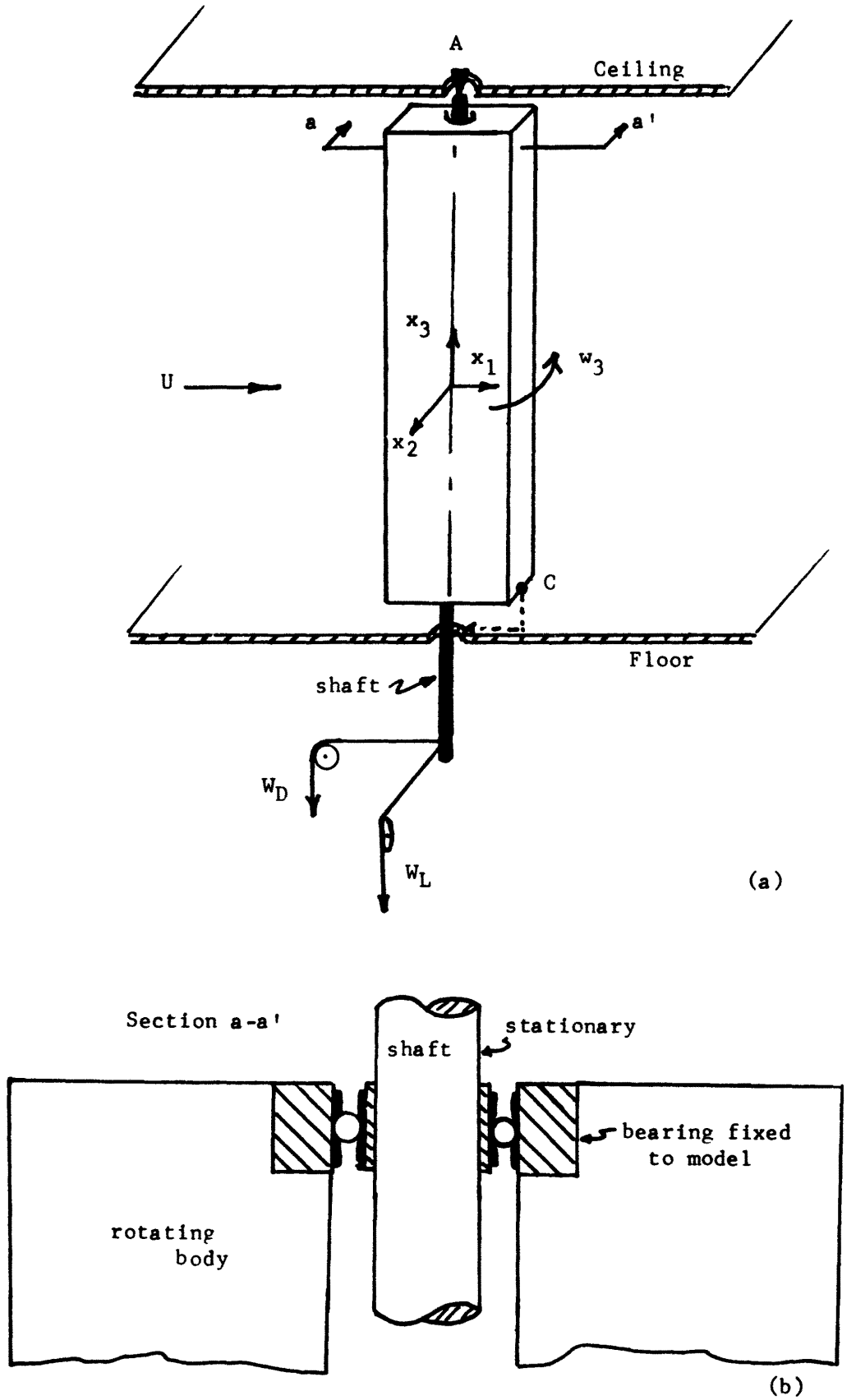

Figure 4.2. Experimental system for autorotational model.

in the x_1 or x_2 directions. Fig. 4.3 shows photographs of the model installed in the tunnel and the universal joint. The shaft on which the model was mounted extended outside the tunnel through a hole in the tunnel floor. The diameter of the hole was only slightly larger than that of the shaft. The end of the shaft was connected to two buckets in which desired weights, W_D and W_L, could be placed to produce moments around the x_1 and x_2 axes, as shown in Fig. 4.2a.

The velocity of the air in the tunnel produced a moment around the x_1 axis proportional to the drag force acting on the body and a moment around the x_2 axis proportional to the lift. These moments acted to deflect the shaft from its vertical position. By applying counter-moments using the weights W_D and W_L, the shaft could be brought back to its original vertical orientation. At that position, the average drag force D was equal to $W_D \cdot \ell_1/\ell_2$, where ℓ_1 and ℓ_2 are corresponding arms from the universal joint to the center of the body and to the point where W_D and W_L acted. Similarly, the average lift L was equal to $W_L \cdot \ell_1/\ell_2$. The natural period of the suspended system, which resembled a pendulum, was approximately two seconds. In the tests the body rotated at a frequency higher than 12 cps. The fluctuations in the forces due to the rotation of the body had the same frequency, and therefore did not produce significant fluctuation of the shaft around the zero deflection point C (see Fig. 4.2a). Using this system, it was possible to determine the values of C_D and C_L to within $\pm$ 10 percent.

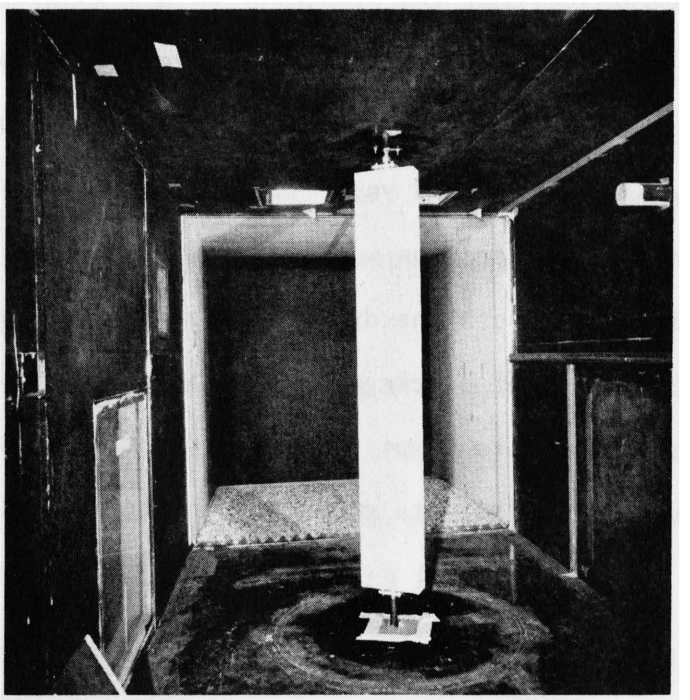

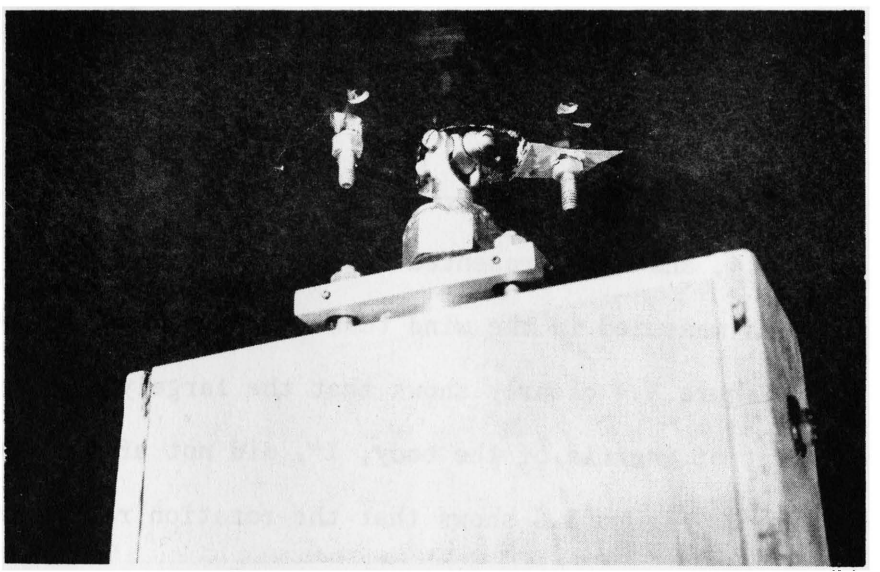

Figure 4.3. Model installed in wind tunnel test section.

The length-to-width ratio of the body was $k = h/b = 6.9$. However, one should realize that the proximity of the tunnel's roof and floor had some effect on the flow near the edges of the body. The ratio t/b of the model was 1/3. The rotating portion of the model was made of wood which gave a value if I^* about 200. The maximum blockage in the test section was 10.7 percent. Such a blockage probably increased both the drag and the lift. However, it was felt that the effect of blockage on $\overline{C}_D$ and $\overline{C}_L$ is within the experimental error and no attempt to correct that data was made. Table 4.1 summarizes the data collected in the wind tunnel tests.

Table 4.1. Experimental Results in the Wind Tunnel Tests.

U (fps)	k	t/b	n (cps)	U/nb	$\overline{C}_D$	$\overline{C}_L$
40	6.88	.33	12.1	4.4	1.74	1.96
50	6.88	.33	15.3	4.3	1.81	1.88

Figures 3.3, 3.4, and 3.10 presented and discussed in Chapter 3 show the data points measured in the wind tunnel tests together with Dupleich's data. Figure 3.4 clearly shows that the largely increased dimensionless moment of inertia of the body, I^*, did not affect the rate of autorotation. Figure 3.3 shows that the rotation rate U/nb of this body is only slightly higher than the rotation rate measured by Dupleich in the water tests for the same value of k.

Note that t/b in the experiments of Dupleich in water was larger than the rest of the experiments (see Table 1, Appendix I).

The slower rotational rate (U/nb larger) in our experiments could be due to the effect of t/b as well as due to the different Reynolds Number and different edge effects.

The lift coefficient corresponding to our experiment is shown together with Dupleich's data in Fig. 3.10. It seems to be only slightly above the rest of the data, probably due to the blockage, or a Reynolds number effect.

The experimental system was also used to examine the stability of the rotational motion of the body. When oriented with its large face normal to the flow, the body was very stable and would hardly oscillate. To induce autorotation it was necessary to give it a strong initial rotation. Once rotation started, it achieved a stable steady state.

Chapter 5

DISCUSSION

We have identified in the previous chapters two possible stable modes of motion of free elongated bodies.

1. Motion without rotation. In such a motion the body is oriented with its large face normal to the relative velocity. This mode appears to be stable for bodies with large dimensionless moments of inertia (I*). The drag coefficient in this case will be of the order of 2. However, if the body is subjected to a large moment around the longitudinal axis or given an initial rotation around that axis, it will start to autorotate.

2. An ideal autorotational mode, with rotation around the longitudinal axis, which is oriented normal to the direction of the relative velocity. The drag coefficient in this case will be reduced and its value could be roughly estimated using the quasi-static approximation. The dimensionelss rotational speed nb/U will be determined primarily by the relative length of $k = h/b$, see Fig. 3.3. Experiments with paper strips suggest that such an orientation is quite stable provided nb/U is large, namely h/b is large, and provided the body is symmetric. This can be easily demonstrated by dropping elongated paper strips (say 1" x 7" strips made of IBM computer cards) after giving them a slight initial

rotation. The motion of such a free falling strip is described in Fig. 5.1a.

However, a slight asymmetry, or a small initial rotation around the x_2 axis will cause a slow w_2 rotation and the body will glide in a helical trajectory, as shown in Fig. 5.1b.

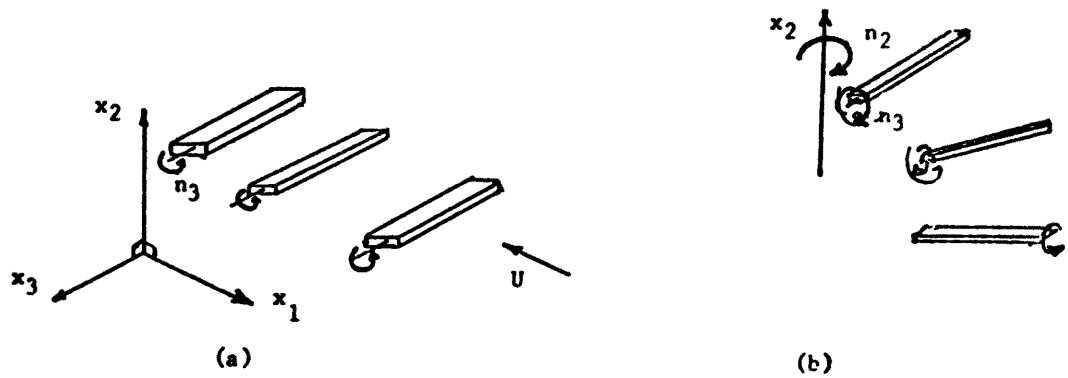

Fig. 5.1. Descents of autorotational bodies.

The effect of the w_2 rotation on the gliding angle, the gliding velocity and the impact of the body when it hits the ground, will be very small. However the trajectory will be drastically different. It should be realized that even in the ideal autorotational case, one cannot determine the trajectory of the body as it will depend on the initial orientation and the direction of rotation. Thus, all one can predict even in this simple case is the area of possible impact and the impact velocity.

Different modes of motion will eventually occur if the bodies are not symmetrical or when autorotation is slow. We shall discuss a few examples:

3. When the center of gravity of the body does not coincide with the center of pressure, rotation around the x_1 axis is generated. Such a rotation might also occur due to initial conditions or a nonuniform velocity field. Observations suggest that once significant autorotation around the longitudinal axis is established, long bodies with slight asymmetry will eventually orient themselves so that the longitudinal axis is horizontal, and glide down in a helical trajectory as shown in Fig. 4.1b.

   On the other hand if the center of gravity is way off to one side, the body will fall down with that side facing the ground as shown in Fig. 5.2a. In this case the drag acting on the body will be the smallest, and the body will have a relatively high speed and impact. Autorotation around the longitudinal axis, which is oriented in this case parallel to the relative velocity will not be sustained.

In an intermediate range, whose limits we cannot define at present, different modes are possible. Various degrees of autorotation will exist together with procession, as shown in Fig. 5.2b.

4. When the cross section of the body normal to the longitudinal axis is circular or close to circular, or when the relative length is small, autorotation might not be maintained or the autorotational speed would be small.

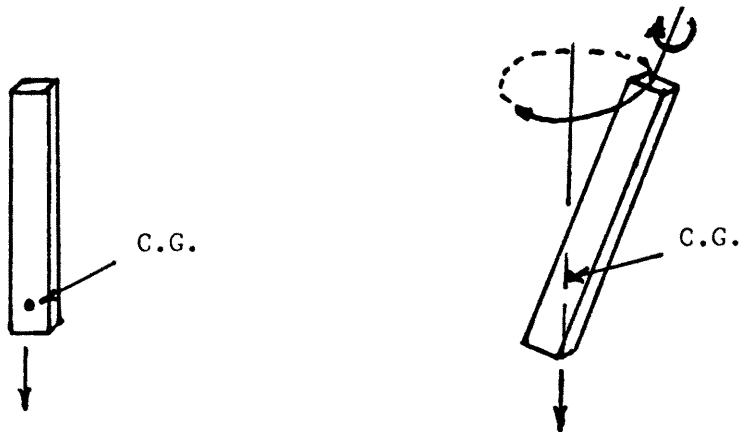

Figure 5.2. Descents of bodies with center of gravity differing from center of pressure.

The stabilizing effect of the autorotation will vanish in this case and the body might orient itself in the non-rotational mode described in paragraph (1) earlier. However, depending on the initial conditions, it could also rotate around any of the axes and exhibit a tumbling motion. In this case the rate of rotation will be small and the average lift forces will be zero. The average drag, which such a tumbling body will experience, could be estimated using the quasi-static approximation. Its value in this case as well as in case (3) will be in between the maximum value obtained when its largest area faces the flow and the minimum value obtained when its minimum area faces the flow.

Many more modes of motion are possible in a nonuniform field or when steady conditions are not achieved.

REFERENCES

1. Dupleich, Paul, Rotation in Free Fall of Rectangular Wings of Elongated Shape, NACA, T.M. No. 1201, 1949.

2. Modi, V. J. and El-Sherbiny, S., "Wall Confinement Effects on Bluff Bodies in Turbulent Flows." Department of Mechanical Engineering, University of British Columbia, 1974.

3. Sadeh, W. Z., "Drag of Tornado-Generated Missiles," Paper presented at the 2nd U.S. National Conference on Wind Engineering Research, Colorado State University, June 1975.

4. Schlichting, H., Boundary Layer Theory (McGraw-Hill, New York, 1968) 6th edition.

5. Simiu, E. and Cordes, M., "Tornado orne Missile Speeds." Institute for Basic Standards, National Bureau of Standards, NBSIR 76-1050, 1976.

6. Smith, A. M. O., On the Motion of a Tumbling Body. Journal of the Aeronautical Sciences, Vol. 20, No. 2, 1953, pp. 73-84.

7. Streeter, V. L., Fluid Mechanics (McGraw-Hill, New York, 1971) 5th edition.

8. Willmarth, W. W., Hawk, N. E., Galloway, A. J., and Roos, F. W., Aerodynamics of Oscillating Disks and Right-Circular Cylinders. Journal of Fluid Mechanics, Vol. 27, Part 1, 1967, pp. 177-207.

Appendix I

DUPLEICH'S DATA

Δ g/dm^2	h (cm)	b (cm)	k	t/b	I*	C_D	C_L	U/nb
1.3	12	2	6	.01	5.2	.96	1.54	4.5
-	9	3	3	-	3.5	1.07	1.15	5.4
-	10	-	3.3	-	-	1.07	1.27	5.0
-	12	-	4	-	-	1.06	1.43	4.5
-	15	-	5	-	-	1.05	1.61	4.1
-	10	4	2.5	-	2.6	1.1	1.08	5.4
-	12	-	3	-	-	1.14	1.29	4.9
-	12	5.2	2.3	-	2.0	1.18	1.20	4.8
-	12	6	2	-	1.73	1.24	1.19	4.8
-	14	-	2.3	-	-	1.17	1.25	4.4
-	16	-	2.6	-	-	1.26	1.51	4.1
-	18	-	3	-	-	1.24	1.62	3.9
-	24	-	4	-	-	1.37	2.18	3.3
-	12	8	1.5	-	1.3	1.37	1.14	4.9
2.04	10.8	3.6	3	-	4.5	.89	.91	5.9
-	14.4	-	4	-	-	.86	1.07	5.1
-	18	-	5	-	-	.88	1.32	4.6
-	15	5	3	-	3.3	.92	1.03	5.4
-	12	6	2	-	2.7	1.0	.86	5.8
-	14	-	2.3	-	-	1.01	1.00	5.5
-	16	-	2.6	-	-	1.00	1.09	5.2
-	18	-	3	-	-	1.00	1.17	4.9
-	24	8	3	-	2.1	1.06	1.30	4.2
-	8	10	.8	-	1.6	1.09	.54	7.4
-	9	-	.9	-	-	1.10	.60	6.9
-	10	-	1.0	-	-	1.11	.64	6.6
-	16	-	1.6	-	-	1.12	.94	5.3
-	20	-	2	-	-	1.13	1.12	4.6
-	25	-	2.5	-	-	1.10	1.27	4.3
-	30	-	3	-	-	1.10	1.44	3.9
2.57	24	8	3	-	2.6	1.2	1.42	4.3
5.14	16.9	5.6	3	-	7.3	.95	.89	5.9
6.32	24	8	3	-	6.3	.96	.96	5.4
7.38	23.8	5.8	4.1	-	10.2	.83	.91	5.7
-	24	8	3	-	7.4	.86	.82	5.6
-	33	15	2.2	-	3.9	.92	.82	5.3
-	40	17	2.4	-	3.5	.94	.9	5.2
7.94	33.5	19.0	1.8	.01	3.3	.91	.71	5.8
8.89	24.0	8.0	3.0	-	8.9	.84	.77	5.7
9.18	6.0	4.0	1.5	-	18.4	.83	.38	9.5
-	6.0	3.0	2.0	-	24.5	.79	.42	9.3
-	10.0	6.0	1.7	-	12.2	.86	.47	7.9
11.5	34.0	8.5	4.0	-	10.9	.86	.96	4.7
+429	7.5	5	1.5	.13	.86	1.17	.93	6.3
-	15	-	3	-	-	1.15	1.61	4.8
-	30	-	6	-	-	1.17	2.53	3.3
+887	5	3.5	1.4	.3	2.53	.87	.55	6.9
-	10	-	2.9	-	-	.85	.92	5.4
-	20	-	5.7	-	-	.86	1.52	4.1
-	30	-	8.6	-	-	.86	2.13	3.3

+ Dupleich's tests with lead and iron in water.

Appendix II

DIMENSIONAL ANALYSIS OF AUTOROTATIONAL MOTION

From the consideration of the problem involved, the rotational rate which an autorotational body will assume is defined by parameters governing the flow such as the fluid velocity, density of the body and the fluid, viscosity and length dimension. Since all of these must be known for a solution to the rotation rate, a functional relationship must exist as shown in Eq. (1).

$$F(n, U, \rho_a, \rho_b, \mu, \ell, \ell_1, \ell_2) = 0 \tag{1}$$

In Eq. (1), n is the rotational rate, ρ_a is the density of the fluid, ρ_b is the density of the body, U is the flow velocity, μ is the viscosity, and ℓ, ℓ_1 and ℓ_2 are various length dimensions.

Using the Buckingham II-theorem one can arrange the above parameters in nondimensional fashion to arrive at the correct functional dependencies. Five II-parameters can be formed using as the repeating variables of U, ρ_a and ℓ as shown in Eqs. (2a-c).

$$II_1 = U^{x_1}\rho_a^{y_1}\ell^{z_1}n \tag{2a}$$

$$II_2 = U^{y_2}\rho_a^{y_2}\ell^{z_2}\mu \tag{2b}$$

$$II_3 = \rho_a/\rho_b \tag{2c}$$

$$II_4 = \ell/\ell_1 \tag{2d}$$

$$II_5 = \ell/\ell_2 \tag{2e}$$

Substituting the dimensions into Eq. (2a), one gets,

$$II_1 = (LT^{-1})x_i(ML^{-3})y_1Lz_1T^{-1}$$

from which the simultaneous equations for x_1, y_1 and z_1 are shown in Eqs. (3a through 3c).

$$x_1 - 3y_1 + z_1 = 0 \tag{3a}$$

$$-x_1 - 1 = 0 \tag{3b}$$

$$y_1 = 0 \tag{3c}$$

From these equation $x_1 = -1$, $y_1 = 0$, $z_1 = 1$, and the first II-term is given by

$$II_1 = \frac{n\ell}{U} \tag{4}$$

Similarly, for Eq. (2b) following the same procedure, the second II-parameter is,

$$II_2 = \frac{\mu}{\rho_a U\ell} = \frac{1}{Re} \tag{5}$$

Since Eqs. (2c, 2d and 2c) are already nondimensional, the functional relation given by Eq. (1) can now be written as

$$f(\frac{n\ell}{U}, \frac{1}{Re}, \frac{\rho_a}{\rho_b}, \frac{\ell}{\ell_1}, \frac{\ell}{\ell_2}) = 0 \tag{6}$$

It should be noted that the nondimensional parameters can be inverted and combined if desired such that Eq. (6) becomes

$$f(\frac{n\ell}{U}, Re, \frac{\rho_b \ell_2}{\rho_a \ell}, \frac{\ell_1}{\ell}, \frac{\ell_2}{\ell}) = 0 \tag{7}$$

In our problem $\ell = b$, $\ell_1 = h$ and $\ell_2 = t$, and rewriting Eq. (7) as

$$\frac{nb}{U} = f_1(Re, I^*, k, t/b), \tag{8}$$

we find the functional relationship of the rotation parameter nb/U depends upon the Reynolds number, dimensionless moment of inertia I^*, aspect ratio k and the thickness to width ratio, t/b.